

Supporting Information for

# **Normalizing Tumor Microenvironment Based on Photosynthetic Abiotic/Biotic Nanoparticles**

Diwei Zheng<sup>§</sup>, Bin Li<sup>§</sup>, Lu Xu, Qiu-Ling Zhang, Jin-Xuan Fan, Chu-Xin Li and  
Xian-Zheng Zhang<sup>\*</sup>

Key Laboratory of Biomedical Polymers of Ministry of Education & Department of  
Chemistry, Wuhan University, Wuhan 430072, P. R. China

<sup>\*</sup> Corresponding author. E-mail: xz-zhang@whu.edu.cn (X.Z. Zhang).

<sup>§</sup> These authors contributed equally to this work.

## Materials and Methods

**Materials.** Teraethylorthosilicate (TEOS), triethanolamine (TEA), stearic acid, AgNO<sub>3</sub>, sodium citrate, acrylamide, MgCl<sub>2</sub>, NaCl, NaOH, CaCl<sub>2</sub>, NH<sub>3</sub>·H<sub>2</sub>O, K<sub>2</sub>CO<sub>3</sub>, NaBH<sub>4</sub>, KMnO<sub>4</sub>, hydroxylamine hydrochloride, N,N-dimethylformamide (DMF), dimethyl sulfoxide (DMSO), sucrose, polyethylene glycol (M.W. = 200) and hexadecyltrimethyl ammonium chloride (CTAC), hexadecyltrimethyl ammonium bromide (CTAB) were obtained from Sinopharm Chemical Reagent Co., Ltd. ZnO nanoparticle (≤ 50nm, 40 w/w in H<sub>2</sub>O), polyethylene glycol (M.W. = 2000), dextran (M.W. = 70000), 1-ethyl-3-(3-dimethylaminopropyl) carbodiimide hydrochloride (EDC·HCl), 4-dimethylaminopyridine (DMAP), hydroxyethyl cellulose, and 30% H<sub>2</sub>O<sub>2</sub> were purchased from Aladdin Reagent Co. Ltd. Methylene blue was obtained from Innochem Reagent Co. Ltd. **FA-PEG<sub>2000</sub>-DSPE was purchased from Ponsure**

**Biotechnology.** Spinach, cabbage and lettuce were purchased from the nearby market. Diisopropylethylamine (DIEA), citric acid, potassium ferricyanide (K<sub>3</sub>Fe(CN)<sub>6</sub>) and urea were purchased from Shanghai Reagent Chemical Co. O-(7-azabenzotriazol-1-yl) uronium hexafluoro-phosphate (HATU) and 7-aza-1-hydroxybenzotriazole (HOAt) were purchased from GL Biochem (Shanghai) Ltd. DSPE-PEG-FA was purchased from Shanghai Ponsure Biotech. Inc. 2',7'-Dichlorofluorescein diacetate (DCFH-DA), pGL6 plasmid and TUNEL cell apoptosis kit were purchased from Beyotime Ltd. ROS-ID™ hypoxia/oxidative stress detection kit was purchased from Enzo Life Sciences Inc. Agarose (low-gel/melting) was obtained from Fisher Scientific. Albumin from bovine serum (BSA) was purchased from Solarbio. N,N-dimethyl-4-nitrosoaniline (RNO) was purchased from TCI. Histidine was purchased from Shanghai REGAL. 4',6-diamidino-2-phenylindole (DAPI), 3-[4,5-dimethylthiazol-2-yl]-2,5-diphenyltetrazolium-bromide (MTT) and

Hoechst 33342 were purchased from Invitrogen Co. Sodium dodecyl sulfonate (SDS) and 2-hydroxyethyl (HEPES) were purchased from Biosharp. 2,2'-azobis[2-imidazolin-2-yl]propane] dihydrochloride and paraformaldehyde was obtained from Acros Organics. Ovalbumin and Rhodamine B were purchased from Sigma-Aldrich.

**Cell Lines.** CT26 cells (ATCC-CRL-2638) was obtained from China Center for Type Culture Collection.

**Antibodies.** CD31 (P2B1), CA-9 (ab184006), HIF- $\alpha$  (H1alpha67),  $\alpha$ -SMA (ab5694) and GLUT-1 (EPR3915) antibodies and FITC conjugated CA-9 antibody were purchased from Abcam Inc.

**Characterization.** Transmission electron microscopy (TEM) images were performed with a JEM-2100 (JEOL) transmission electron microscope. Zeta potential and particle size were studied by using a zeta sizer (Nano ZS, Malvern Instruments). UV-vis spectra were measured with a Lambda 35 UV/VIS Spectrometer (Perkin-Elmer). Fluorescence spectra were performed with a RF-5301PC spectrofluorophotometer (SHIMADZU). Dissolved oxygen was measured with a JPSJ-605 (INESA) oxygen dissolving meter. *In vitro* cell imaging and *ex vivo* 3D reconstruction imaging CT were performed with UltraVIEW VoX spinning disk confocal microscope. Scanning was performed in Quantum FX micro-CT (Perkin-Elmer).

**Synthesis of Stearic Acid Conjugated  $\beta$ -Cyclodextrin.** 200 mg ethanediamine- $\beta$ -CD (0.17 mmol) and 96.6 mg stearic acid (0.34 mmol) were dissolved in 12 mL DMF/DMSO (v/v = 1:1). The mixture of HATU (212.6 mg, 0.56 mmol), HOAt (76.1 mg, 0.56 mmol) and DIEA (204  $\mu$ L, 1.17 mmol) were dissolved in 2 mL DMF, and add into above solution under stirring. After that, the reaction was kept at 35  $^{\circ}$ C for 6 h. The product was precipitated in 10 times volume of acetone and centrifuged, then washed for 5 times with acetone and dried under vacuum.

**Synthesis of SiO<sub>2</sub> Nanoparticle.** 20 g CTAC and 0.8 g TEA were dissolved in 200 mL of DI water and stirred for 1 h at 95  $^{\circ}$ C. 15 mL TEOS (15 mL) was added dropwise into the solution and the reaction was kept at 95  $^{\circ}$ C for another 1 h. The SiO<sub>2</sub> nanoparticle was subsequently obtained through centrifugation and washed with DI water/methanol for 3 times.

**Synthesis of Au Nanoparticle (AuNP).** 50 mL 0.01% HAuCl<sub>4</sub> was mixed with 0.25 mL 0.2 mol/L K<sub>2</sub>CO<sub>3</sub> aqueous solution. Then, 1 mL 0.5 mg/mL NaBH<sub>4</sub> was added dropwise under stirring. When the solution color turned into wine red, keep stirring for 3 min. The final solution was stored at 4  $^{\circ}$ C for immediate use.

**Synthesis of CaO<sub>2</sub> Nanoparticle.** 800  $\mu$ L 100 mg/mL CaCl<sub>2</sub> was mixed with 50 mL Polyethylene glycol (M. W. = 200) and 400  $\mu$ L 1 M NH<sub>3</sub>·H<sub>2</sub>O with at 400 rpm. 400  $\mu$ L 30% H<sub>2</sub>O<sub>2</sub> was added into the solution dropwise. After keeping stirring for 5 h, pH of the solution was adjusted by 1 M NaOH to 11.5. The production was obtained by 11000 rpm centrifugation and washed by NaOH (pH = 13), DI water and ethanol in order, and then stored in ethanol.

**Synthesis of MnO<sub>2</sub> Nanoparticle.** 0.5 g KMnO<sub>4</sub>, 0.11 g CTAB and 5.5 g PEG2000 were dissolved in 60 mL DI water. After completely dissolved, the solution was treated with ultrasound in 80% power for 20 min. The production was obtained through centrifugation and washed by DI water and ethanol for 3 times each, and then dried at 60 °C overnight.

**Synthesis of Rhodamine B (RhB)-Conjugated Dextran.** 500 mg dextran (M. W. = 70000, 0.007 mmol) was dissolved in 10 mL PBS 34 mg (0.07 mmol) RhB was mixed with 16 mg (0.08 mmol) EDC HCl and 10.4 mg (0.08 mmol) DMAP in 5 mL PBS. After 30 min stirring, the RhB mixture was added into dextran solution and keep stirring for 24 h. Then, the production was purified by dialysis and dried by lyophilization.

**SDS Page.** Tk and leaf homogenate were dispersed in lithium dodecyl sulfate. Then, the loading buffer (Invitrogen) was heated to 90 °C for about 10 min. After that, 20 µL samples were loaded into each well of a NuPAGE Novex 4-12% Bis-Tris minigel. 3-(N-morpholino) propane sulfonic acid and sodium dodecyl sulfate (Invitrogen) were used as running buffer in an XCellSureLock electrophoresis system. By using Coomassie blue (Invitrogen), protein staining was accomplished. After destained in water overnight, protein was transferred to Protran nitrocellulose membranes (Whatman) using an XCell II Blot Module (Invitrogen) in NuPAGE transfer buffer (Invitrogen). Membranes were probed with different markers films were developed by using ECL western blotting substrate (Pierce) in a Mini-Medical/90 developer (ImageWorks).

**Fluorescent Quenching of Tk Coated AuNP.** Tk coated AuNP was prepared as the same method as Tk coated AgNP except using as prepared AuNP. 1 mL of Tk coated AuNP was mixed with 10 mg of albumin from bovine serum (BSA) as quenching group. The simple mixture of 0.5 mL Tk, 0.5 mL AuNP ( $1 \text{ mg mL}^{-1}$ ) and 10 mg of BSA was set as control group. 0.5 mL Tk solution mixed with 0.5 mL PBS was used as blank. The fluorescence intensity of these three groups was collected with a wavelength from 650 nm to 750 nm under 480 nm excitation and divided by each concentration of chlorophyll for normalization.

**ROS Production Assay.** The ROS production of materials was tested by using RNO method. Briefly, the test solution contained 100  $\mu\text{L}$  PLANT + MB solution, 50  $\mu\text{L}$  RNO (500  $\mu\text{M}$ ), 100  $\mu\text{L}$  histidine (90  $\mu\text{M}$ ) and 750  $\mu\text{L}$  DI-water. The absorbance of the solution was measured at 440 nm every one minute after LED light (660 nm, 18 W) irradiation. In control group, DI-water was replaced by 1 mM hydroxylamine hydrochloride aqueous solution. The dissolved oxygen was exhausted by sponge iron  $\text{O}_2$  eliminating device for hypoxia groups.

**Glucose and Lactate Concentration.** The extracellular glucose concentration was measured with ACCU-CHEK glucometer (Roche, USA). At different time points, 5  $\mu\text{L}$  of medium was collected, and the glucose concentration was measured. Lactic acid concentration was determined by a lactate assay kit (Jiancheng, Nanjing, China) based on lactate dehydrogenase. At different time points, the culture medium was used for measuring the extracellular lactate concentration.

**Wound Healing Assay.** The wound-healing assay was used to study the migratory ability of CT26 cells with and without PLANT treatment. Briefly, CT26 cells were seeded to be 70-80% confluent, and then a pipette tip was used to remove cells with a line. CT26 co-incubated with  $50 \mu\text{g mL}^{-1}$  of PLANT for 4 h and then exposed to 660 nm LED light. Cells were photographed using inverted fluorescence microscope at different time points and the distance of wound was analyzed with ImageJ.

***In Vivo* Animal Experiment.** All animal experiments were performed according to guidelines for laboratory animals established by the Wuhan University Center for Animal Experiment/A3-Lab. All study protocols were approved by the Institutional Animal Care and Use Committee (IACUC) of the Animal Experiment Center of Wuhan University (Wuhan, China). Female Balb/c mice were purchased from Liaoning Changsheng Biotech. co. LTD.

**DCFH-DA Assay.** CT26 cells were seeded in a 35 mm culture dish with a density of  $1.0 \times 10^5$  and then incubated in 1 mL 1640 medium containing 10% FBS. 24 h after seeding, PLANT + MB or free MB (with MB concentration of  $1 \mu\text{g mL}^{-1}$ ) were added. 6 h later, 1 mL 1640 medium containing DCFH-DA ( $10 \mu\text{M}$ ) was added and 660 nm light irradiation ( $30 \text{ mW cm}^{-2}$ , 2 min) was performed subsequently. The green fluorescence in CT26 cells was observed with a wide-field fluorescence microscopy.

**Intracellular Hypoxia Measurement.** CT26 cells were seeded in a 35 mm culture dish with a density of  $1.0 \times 10^5$  and then incubated in 1 mL of 1640 medium containing 10% FBS. 24 h after CT26 cells were seeded, PLANT + MB or free MB

(with MB concentration of  $1 \mu\text{g mL}^{-1}$ ) was added. 6 h later, 0.2  $\mu\text{L}$  Hypoxia Red Detection Reagent was added and 660 nm light irradiation ( $30 \text{ mW cm}^{-2}$ , 2 min) was performed. The red fluorescence in CT26 cells was observed with a wide-field fluorescence microscopy 30 min after the irradiation.

***In Vitro* TUNEL assay.** CT26 cells were seeded in a 35 mm culture dish with a density of  $1.0 \times 10^5$  and then incubated in 1 mL 1640 medium containing 10% FBS. 24 h after CT26 cells were seeded, PLANT + MB or free MB with different concentration were added. 6 h later, 660 nm light irradiation ( $30 \text{ mW cm}^{-2}$ , 2 min) was performed on CT26 cells. After 24 h of co-incubation, apoptotic cells were stained with TUNEL assay according to the vendor's instruction. The fluorescence in CT26 cells was analyzed with a wide-field fluorescence microscopy.

***In Vivo* Tumor Targeting Ability of PLANT.** To study the *in vivo* tumor targeting ability of PLANT, 100  $\mu\text{L}$  of PLANT + PLANT or PLANT + MB without FA was *i.v.* injected into CT26 tumor bearing mice. 15 min, 1 h, 2 h, 4 h, 6 h, 12 h and 24 h post-injection, the *in vivo* bio-distribution of each material was observed with IVIS spectrum imaging system. 24 h after the injection, 3D fluorescent reconstruction imaging with a transluminal model. The structural information of mice was collected with a  $\mu\text{-CT}$  and overlaid with 3D fluorescent images.

**CLARITY Technique for Tissue Clearing.** PLANT + MB or MB (with a MB dose of  $5 \text{ mg kg}^{-1}$ ) was *i.v.* injected into CT26 tumor bearing mice. 24 h post-injection, 660 nm laser irradiation ( $155 \text{ mW cm}^{-2}$ , 2 min) was performed. Mice were anesthetized and sacrificed 24 h after the irradiation. Then, mice were transcardially perfused with

ice-cold PBS containing 0.5% (w/v)  $\text{NaNO}_2$  and  $10 \text{ U mL}^{-1}$  heparin. When the perfusate drains were clear, the perfusion was stopped. Tumors were collected and post-fixed with 4% paraformaldehyde for 2 h on a water baths shaker at  $37^\circ\text{C}$ . Tumor samples were then soaked in ice-cold PBS containing acrylamide monomer 4% (w/v) and 2, 2'-azobis [2-imidazolin-2-yl) propane] dihydrochloride thermoinitiator (0.25% (w/v) at  $4^\circ\text{C}$  for 1 d. The polymerization of hydrogel was initiated by placing the above system in a  $37^\circ\text{C}$  water bath for 3 h under  $\text{N}_2$  protection. The as prepared hydrogel/tumor hybrid was delipidated with 10% SDS contained PBS on a water baths shaker at  $37^\circ\text{C}$  for 3 d. Further staining could be performed on the obtained semitransparent tissue hydrogel. To mark the nucleus, the tissue hydrogel was immersed in DAPI solution for 2 d and then washed with PBS for another 2 d. The cleared tissue could be incubated in PBS containing 1:200 FITC labeled CA-9 antibody for 4 d at  $37^\circ\text{C}$  to mark hypoxic regions within the tumor. Besides, 4 d of co-incubation with 1:1 TUNEL staining solution could also label apoptotic cells within the tumor.

**Large-Scale 3D Fluorescence Mapping of Transparent Tissue.** 1 d before the imaging, the tissue hydrogel was immersed in histodenz solution with a refractive index of 1.47, and the hydrogel would become optically transparent within few hours. Z-scanning of tissue hydrogel was performed with a spinning disk confocal microscope. The depth of Z-scanning imaging could be  $500 \mu\text{m}$  and the step-size is  $1 \mu\text{m}$ . A  $1300 \mu\text{m} \times 1300 \mu\text{m}$  area could be scanned for one time. The VAA-3D TeraFly software was used for the 3D volumetric visualization of images.

**Distribution of PLANT among Tumor Tissue.** PLANT + MB (with a MB dose of 5 mg kg<sup>-1</sup>) was *i.v.* injected into CT26 tumor bearing mice. 24 h post-injection, mice were anesthetized and sacrificed. Mice tumors were collected and fixed with 4 % paraformaldehyde for 48 h. Morphology of tumors were scanned in a high-resolution  $\mu$ -CT system. After that, tumors were cut into slices with equal intervals. The intensity of *E. coli* fluorescence was calculated with ImageJ software.

**2-DG 750, Cy7-Conjugated T-Lectin and RhB-Conjugated Dextran.** The glycometabolism capacity of CT26 tumor bearing mice after different treatments was imaged with Xenolight RediJect 2-DG 750 (PerkinElmer, USA). Briefly, mice in both groups were injected with the probe, and then underwent fluorescence imaging at 6 and 24 h after probe injection. Cy7-conjugated T-lectin was used to study the tumor angiogenesis after each treatments. After various treatments, 2 nmol (100  $\mu$ L) of Cy7-conjugated T-lectin was *i.v.* injected into mice. The *in vivo* imaging was performed 6 h after post-injection. Vessel leakage was analyzed after intravenous injection of 0.25 mg rhodamine B-conjugated dextran 70 kDa. For *ex vivo* fluorescence imaging, 10 min after the injection, mice were perfused with saline and 2% PFA. Tumors were then harvested and frozen in optimum cutting temperature compound. For *in vivo* study, the *in vivo* dextran accumulation was visualized 6 h after post-injection.

***In Vivo* ROS Generation Kinetic Study.** Firefly luciferase sequence and PEST degran were added to pARE-luc vector (Beyotime) with pGL6 backbone. Destabilized luciferase reporter was constructed by inserting firefly luciferase with PEST from pGL4.41 vector. CT26 cells were stably transfected with the as-prepared

plasmid using Lentivirus (Thermo Fisher Scientific) according to the manufacturer's instructions, and neomycin ( $80 \text{ mg mL}^{-1}$ ) was added. To determine the ROS driven bioluminescence of CT26<sup>OR</sup> cells, a SpectraMax i3x multi-mode detection platform (molecular device) was used. After PLANT + MB treatment with different dose ( $0.25 \text{ }\mu\text{g mL}^{-1}$ ,  $0.5 \text{ }\mu\text{g mL}^{-1}$ ,  $1 \text{ }\mu\text{g mL}^{-1}$ ,  $2 \text{ }\mu\text{g mL}^{-1}$ ) and different light irradiation time (10 s, 30 s, 60 s and 120 s), D-luciferin was added (with a final concentration of  $150 \text{ }\mu\text{g mL}^{-1}$ ) and the bioluminescence intensity was measured.

To determine the *in vivo* ROS generation of PLANT + MB,  $100 \text{ }\mu\text{L}$  of CT26<sup>OR</sup> cells ( $1 \times 10^6$  cells per mouse) were subcutaneous injected into the back of female Balb/C mice. When the mice tumor volumes grown approximated to  $200 \text{ mm}^3$ ,  $100 \text{ }\mu\text{L}$  of Ag or free MB (with a MB concentration of  $5 \text{ mg kg}^{-1}$ ) was *i.v.* injected into tumor bearing mice ( $n = 4$ ). 24 h after the injection,  $100 \text{ }\mu\text{L}$  of D-luciferin ( $3 \text{ mg per mice}$ ) was intraperitoneal injected into mice and  $660 \text{ nm}$  laser irradiation ( $155 \text{ mW cm}^{-2}$ , 2 min) was then performed. The *in vivo* bioluminescence was determined with IVIS spectrum imaging system.

**Immunofluorescent Staining.** Tumor samples were collected, washed with cold PBS and stored at  $-80 \text{ }^\circ\text{C}$ . Tissue slices were prepared with a Leica microsystems VT1200S. After blocking non-specific binding site in samples with 10% FCS, tumor sections were stained with CD31, CA-9 and HIF- $\alpha$  primary antibodies for 2 h. Then, samples were washed with 10% FCS for 3 times, and FITC or Alexa Fluor594 labeled secondary antibodies (Molecular Probes-Life Technologies Inc) ( $5 \text{ }\mu\text{g mL}^{-1}$ ) were also added and stained for another 2 h. Samples were then washed with 10% FCS for 3 times. Nuclei were stained with  $10 \text{ }\mu\text{M}$  DAPI. Coverslides were mounted with

Fluoromount-GTM medium (Southern Biotechnologies). Sections were observed with a wide-field fluorescence microscopy.

**Blood IgE Concentration Measurement.** Female Balb/C mice were intraperitoneal injected with ovalbumin, PLANT or Tk with a dose of 5 mg kg<sup>-1</sup> (n = 4). 10 days later, another intraperitoneal injection of various materials was also performed. 24 h after the 2nd injection, blood samples were collected from heart and serum and then isolated. The IgE concentration within serum was analyzed with IgE-specific ELISA kits (Proimmune) according to the vendor's instruction. The mean value of three independent experiments was carried out.

**Statistical Analysis and Sample Collection.** Unless indicated otherwise, 'center values' was defined as mean, and the error bars in each figure represent S.D. of at least three independent experiments measured. For statistical analyses, two-tailed Student's t-tests were performed by using Microsoft Excel 2013. Significance among more than two groups was calculated using ANOVA Turkey's test by using SPSS 18.0. \* $P < 0.05$ , \*\* $P < 0.01$ , \*\*\* $P < 0.001$ . A P value of less than 0.05 was considered as statistically significant. For all cell experiments, data were collected from at least 6 independent experiments. For cell experiments and *in vivo* experiments, investigators performing operations were blinded to treatment groups. In *in vivo* experiments, animals were randomly divided into different groups.

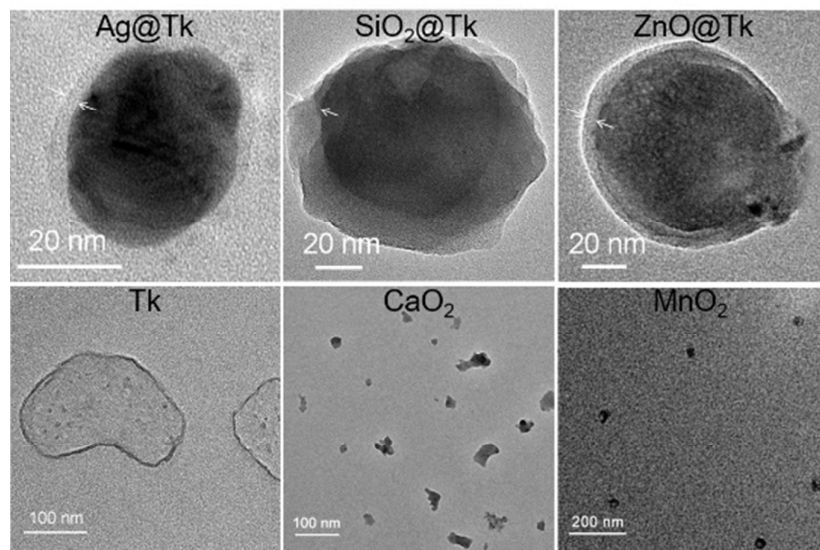


**Figure S1.** TEM image of PLANT, thylakoid isolated from spinach leaves, CaO<sub>2</sub> and MnO<sub>2</sub>.

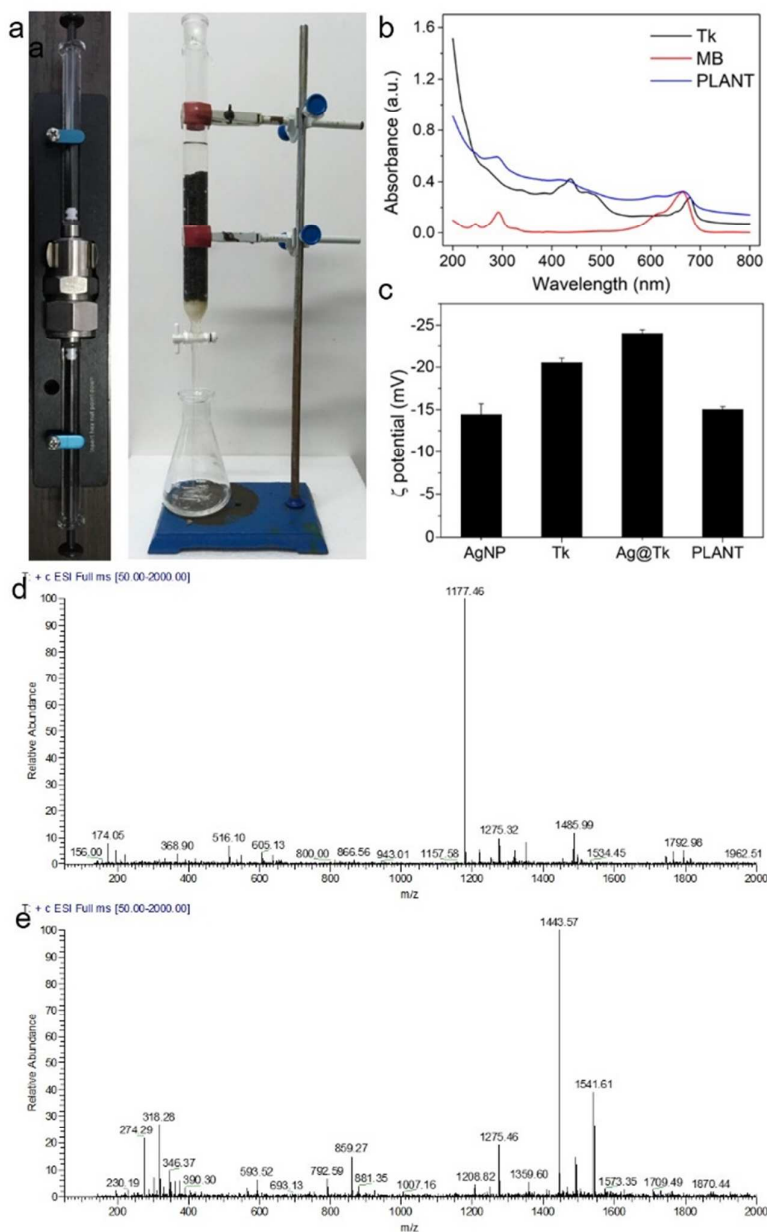


**Figure S2.** *In vitro* study of PLANT. **a.** Photos of Avanti miniextruder (left) and sponge iron O<sub>2</sub> eliminating device (right). **b.** UV-vis absorption spectra of Ag@Tk, Ag@MBTk and PLANT. **c.** Zeta potential of diverse materials. **d.** ESI spectrum of ethanediamine-β-CD (calcd for C<sub>44</sub>H<sub>77</sub>N<sub>2</sub>O<sub>34</sub><sup>+</sup>: 1177.07; found 1177.53). **e.** ESI spectrum of stearic acid conjugated β-cyclodextrin (calcd for C<sub>62</sub>H<sub>111</sub>N<sub>2</sub>O<sub>35</sub><sup>+</sup>: 1443.54; found 1443.58).

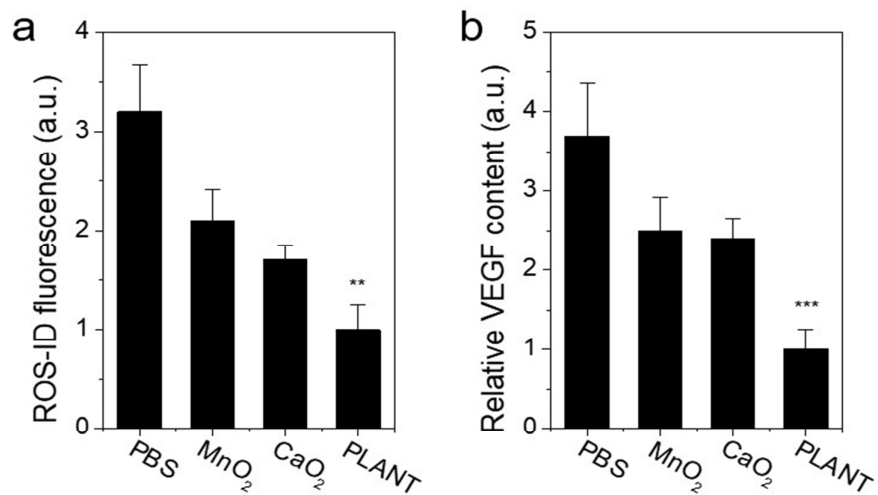


**Figure S3.** Quantitative analysis of ROS-ID fluorescence and VEGF content. **a.** Quantitative analysis of surface plot images of ROS-ID stained CT26 MTS after 4 h co-incubation with PBS, MnO<sub>2</sub>, CaO<sub>2</sub> and PLANT. **b.** VEGF elisa analysis for the relative VEGF content of CT26 MTS after 4 h co-incubation with PBS, MnO<sub>2</sub>, CaO<sub>2</sub> and PLANT.

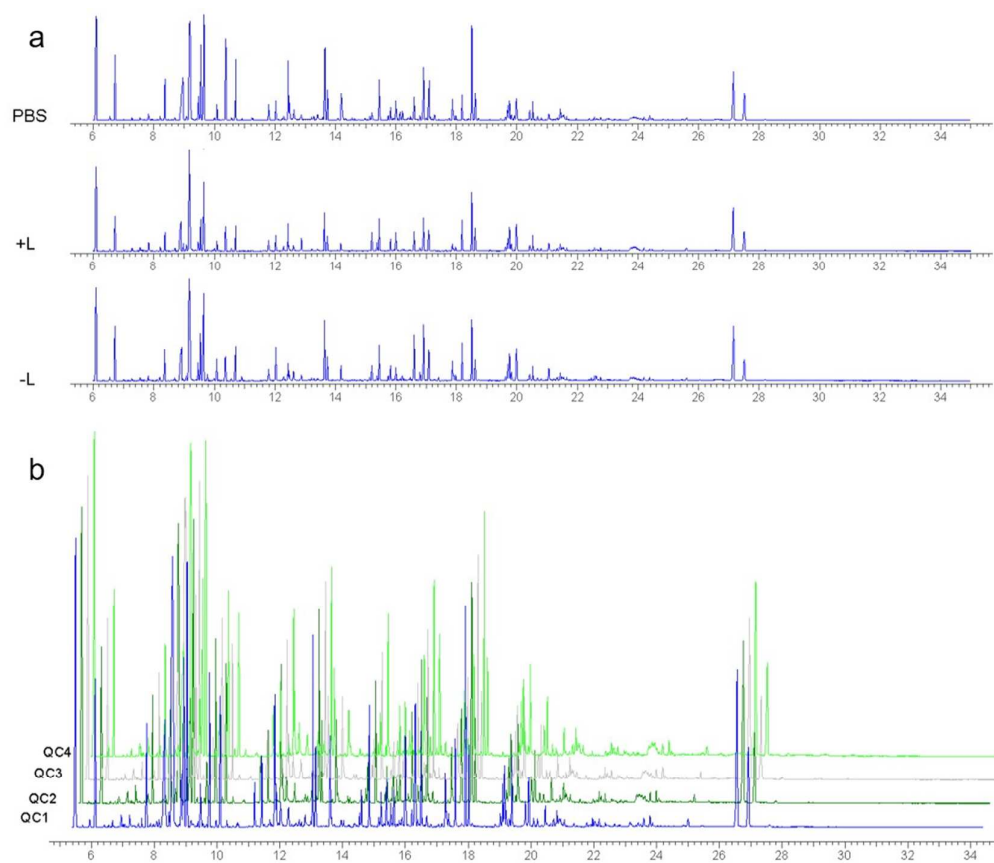


**Figure S4.** GC-MS based metabolomics analysis of PLANT treated mice tumor. **a.** Representative ion chromatography of GC-MS analysis. **b.** Total ion chromatography of GC-MS analysis.

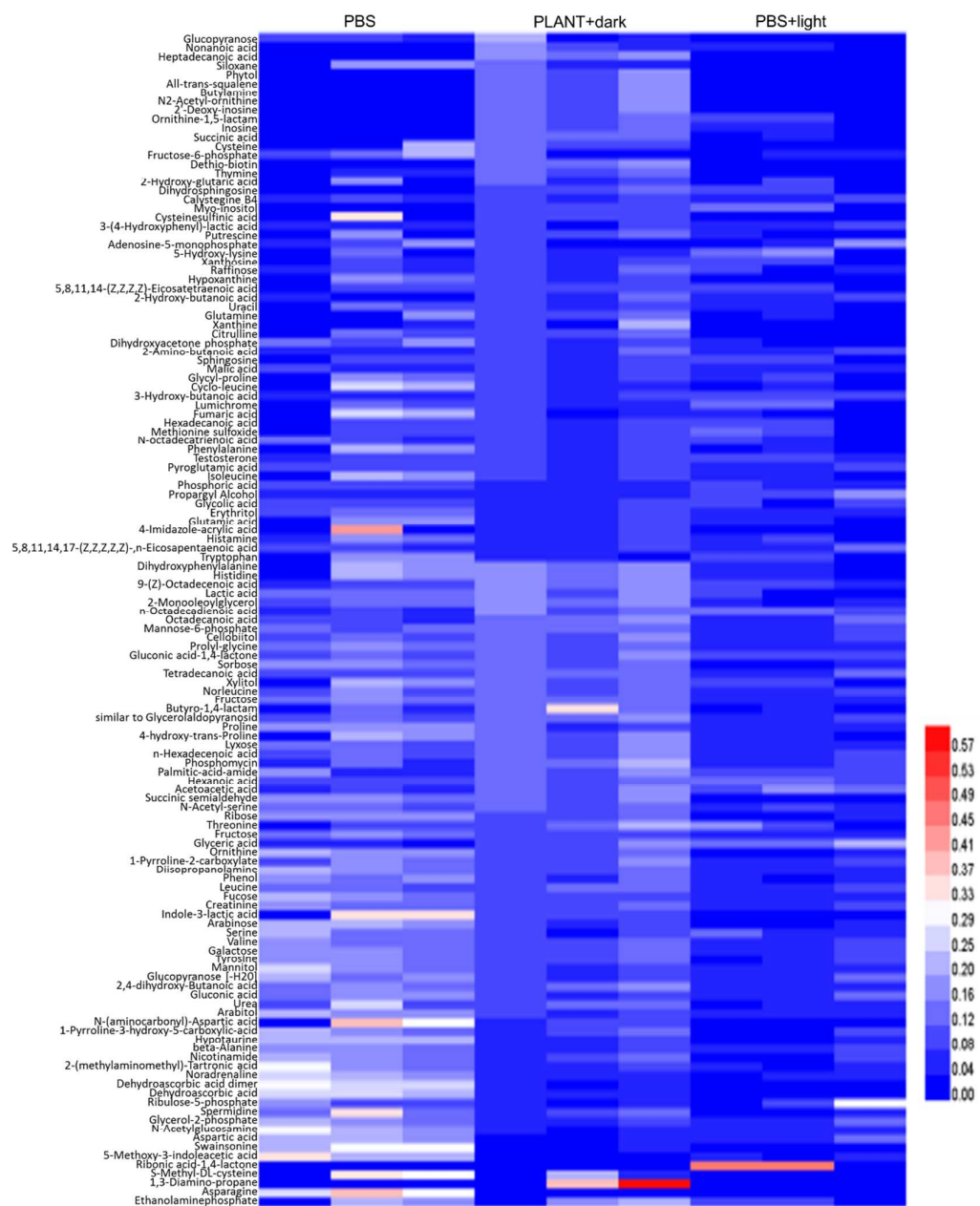


**Figure S5.** Heatmap representation of metabolite intensities. Metabolites showed a significant correlation between PBS, PLANT + light and PLANT + dark groups. The relative abundance of each metabolite is color coded as indicated in the figure legend.

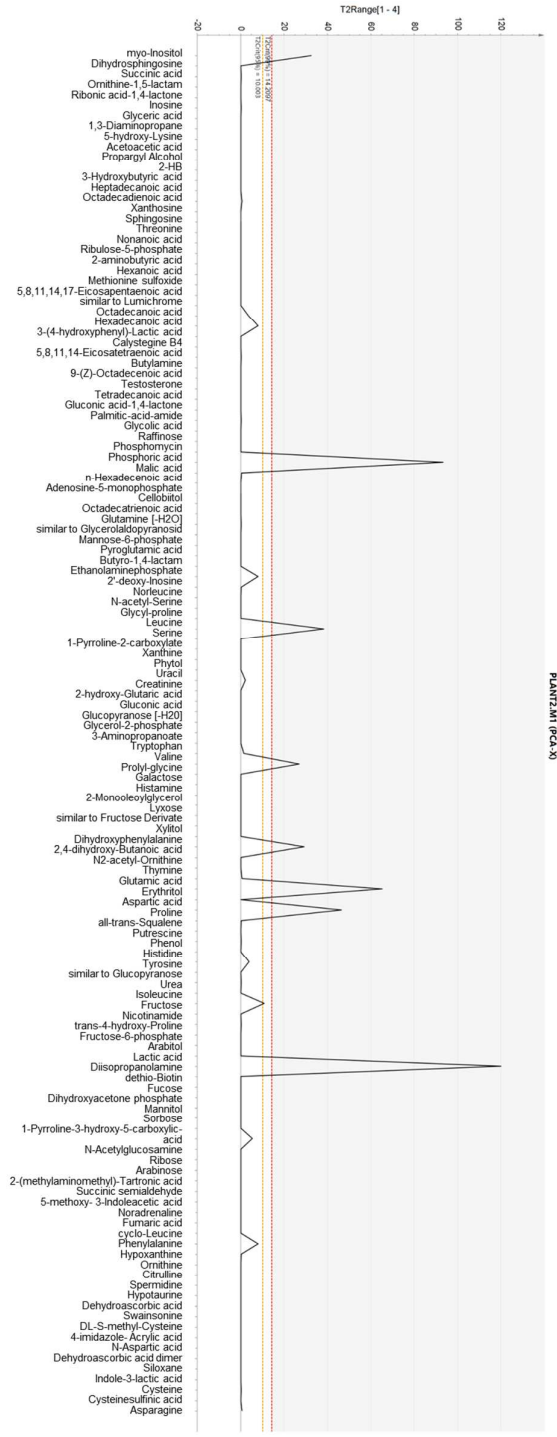


**Figure S6.** Hotelling's trace multivariate t-test of all differential metabolites.  $T^2$  statistics with a 95% and 99% confidence regions were calculated based on all differential metabolites.

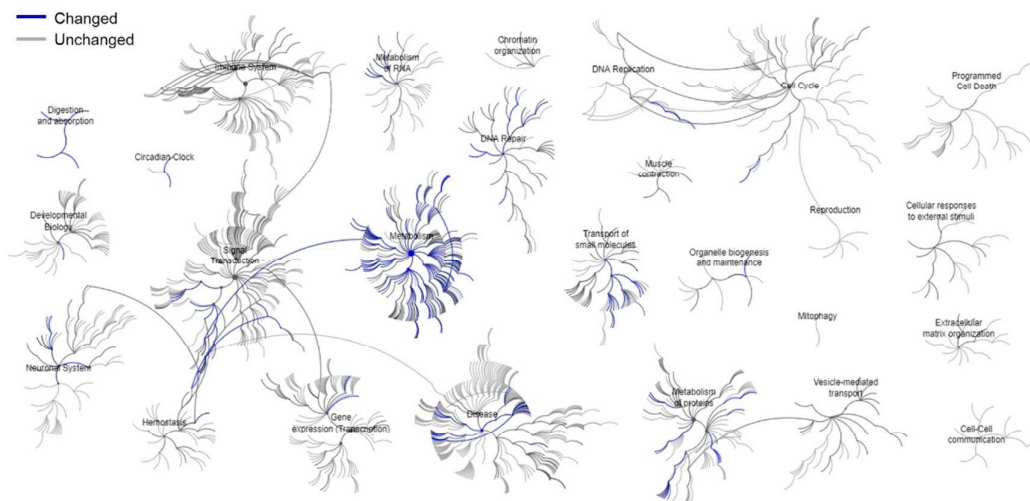


**Figure S7.** The Reaction map shows the reactions annotated in Reactome. PLANT treatment associated pathway was highlighted in blue, whereas unchanged pathway was colored with gray. The reaction clusters of top-level processes were presented.

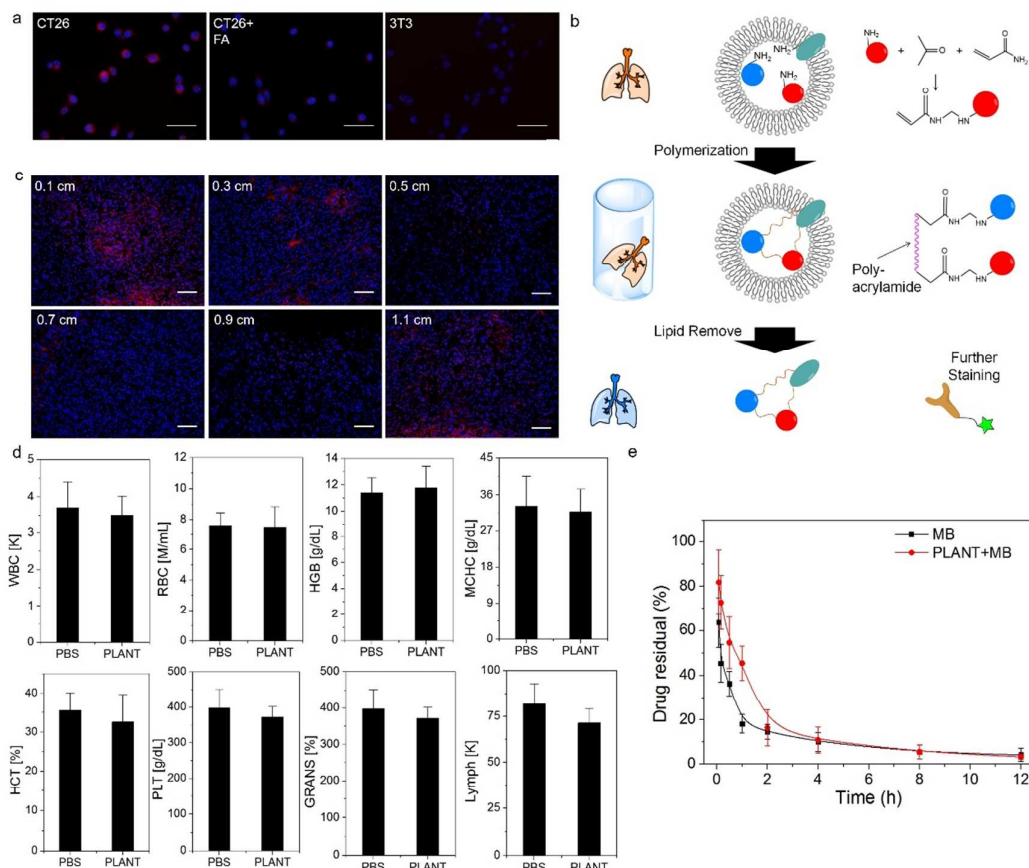


**Figure S8.** Biosafety and targeting performance of PLANT. **a.** *In vitro* cellular uptake study of PLANT of folate receptor positive CT26 cells, CT26 cells + free folic acid and folate receptor negative 3T3 cells (scale bar 50  $\mu\text{m}$ ). As compared with 3T3 cells, CT26 cells endocytosed more PLANT. The free folic acid treatment significantly suppressed the internalization of PLANT. **b.** Schematic illustration of the Clarity tissue-clearing method. First, mice tumor is cross-linked by paraformaldehyde (red) in the presence of acrylamide monomers (blue). The C=C double bond is added to amino contained macromolecules *via* schiff base. After the initiating of polymerization, covalently linking macromolecules to monomers are polymerized into a hydrogel mesh. SDS pulls out lipid molecules from the tissue, whereas leaving crosslinked biomolecules in place. **c.** *Ex vivo* fluorescence imaging of mice tumor with different depth. 100  $\mu\text{L}$  of PLANT + MB or free MB (with a MB dose of 5 mg

kg<sup>-1</sup>) was *i.v.* injected into mice. 24 h after the injection, mice tumors were collected, fluorescence of PLANT at different depths was studied (scale bar 200 μm). **d.** Blood routine examination of mice after *i.v.* injection of PLANT + MB. 100 μL of PLANT + MB or free MB (with a MB dose of 5 mg kg<sup>-1</sup>) was *i.v.* injected into mice. 48 h after the injection, biochemical indexes of liver and kidney toxicity was measured with a MC6200 VET automatic blood cells analyzer. **e.** Pharmacokinetics study of PLANT. 100 μL of PLANT + MB or free MB (with a MB dose of 5 mg kg<sup>-1</sup>) was *i.v.* injected into mice. At different time point, 10 μL of blood was collected, and the fluorescence intensity of each blood sample was measured with a fluorescence spectrophotometer.

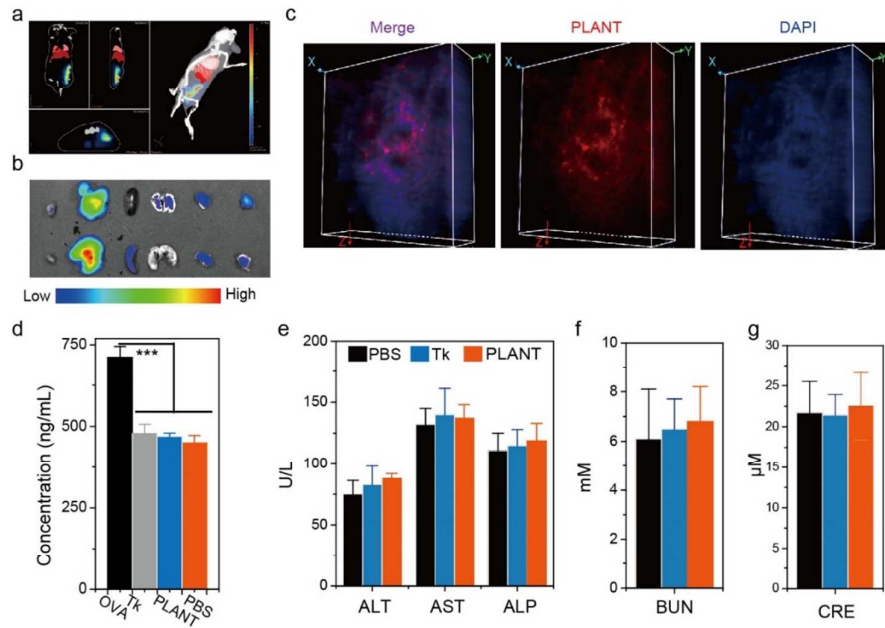


**Figure S9.** *In vivo* tumor targeting ability and biosafety of PLANT. **a.** 3D reconstructed *in vivo* fluorescence imaging 24 h after the *i.v.* injection of PLANT. **b.** *Ex vivo* fluorescence imaging of heart, liver, spleen, lung, kidney and tumor 24 h after the *i.v.* injection of PLANT (up) and PLANT without folic acid, respectively. **c.** A 1.3 mm  $\times$  1.3 mm  $\times$  0.3 mm cube of 3D reconstructed image of CLARITY treated tumor tissues. **d.** IgE concentrations after two doses of instillation with PLANT (20 mg kg<sup>-1</sup>), Tk (20 mg kg<sup>-1</sup>) and OVA (40 mg kg<sup>-1</sup>). **e-g.** Blood biochemistry data of liver and kidney function markers including alanine transaminase (ALT), aspartate transaminase (AST), alkaline phosphatase (ALP), blood urea nitrogen (BUN) and creatine (CRE). The blood biochemistry analysis was performed 24 h after the *i.v.* injection of PLANT (20 mg kg<sup>-1</sup>) and Tk (20 mg kg<sup>-1</sup>). Significance between every two groups was calculated using unpaired two-tailed Student's t test. \* $P < 0.05$ , \*\* $P < 0.01$ , \*\*\* $P < 0.001$ . The mean values and S.D. are presented.

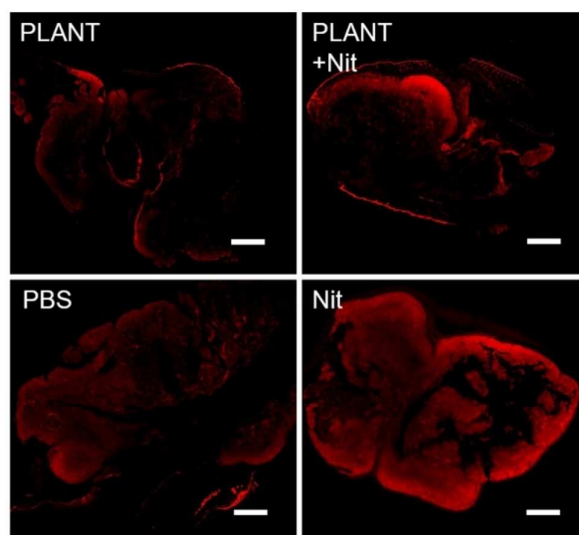


**Figure S10.** *Ex vivo* fluorescence mapping of GLUT1 distribution. Fluorescent mapping and false color fluorescent mapping of GLUT-1 distributions among the tumor tissue 48 h after treated with Nit ( $125 \text{ mg kg}^{-1}$ ), PLANT ( $20 \text{ mg kg}^{-1}$ ) and PLANT + MB ( $20 \text{ mg kg}^{-1}$ ) (scale bar:  $1000 \mu\text{m}$ ).

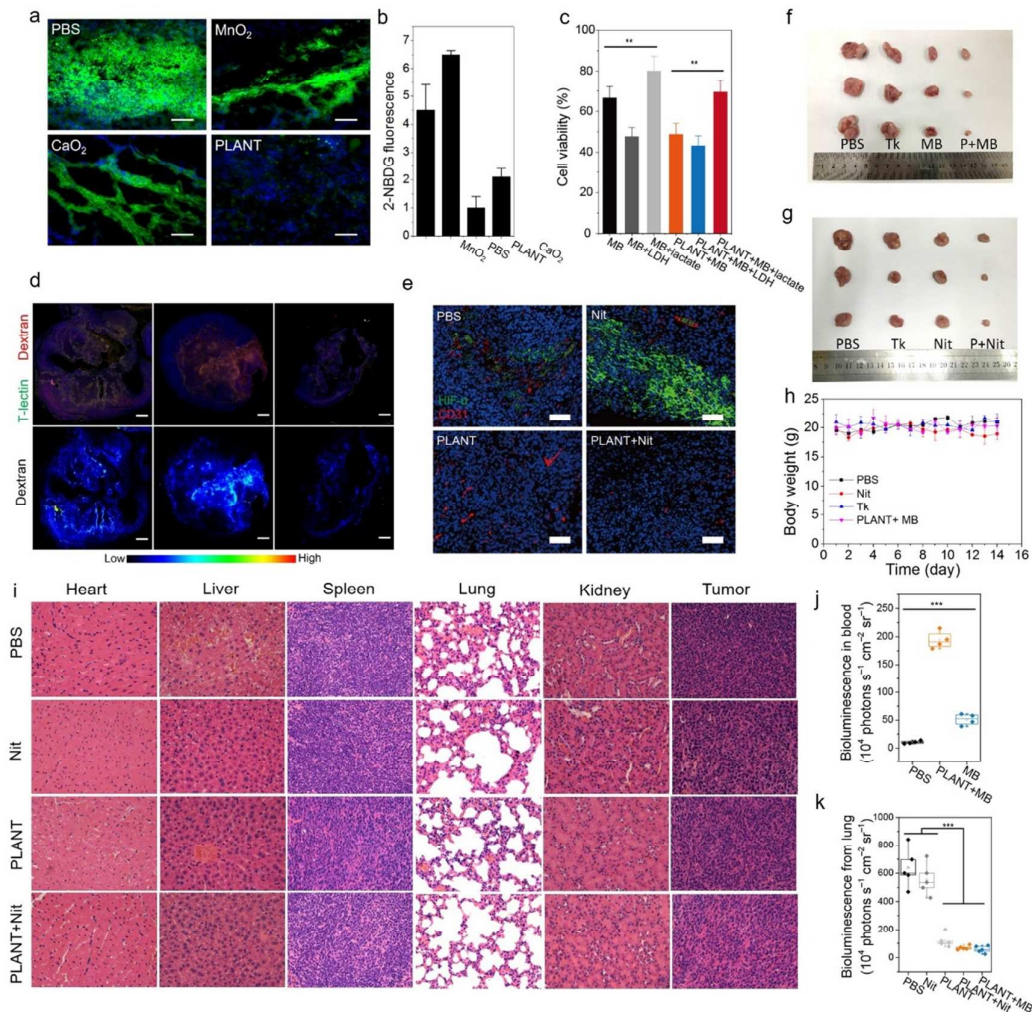


**Figure S11.** The therapeutic effect of PLANT combined with anti-angiogenesis therapy in inhibiting CT26 tumor growth. **a.** Fluorescence imaging of 2-NBDG accumulation within PBS, MnO<sub>2</sub>, CaO<sub>2</sub> or PLANT treated mice tumor (scale bar: 100 μm). **b.** Quantitative analysis of the 2-NBDG fluorescence within PBS, MnO<sub>2</sub>, CaO<sub>2</sub> or PLANT treated mice tumor. **c.** Cell viability assay of CT26 cells after treated with PLANT (5 μg mL<sup>-1</sup>, irradiated with 660 nm LED light for 10 min) and free MB (1 μg mL<sup>-1</sup>, irradiated with 660 nm LED light for 10 min) in both normoxic and hypoxic environments. **d.** Fluorescent mapping and false color fluorescent mapping of 2-NBDG micro-distributions among the tumor tissue 48 h after treated with Nit (125 mg kg<sup>-1</sup>), PLANT (20 mg kg<sup>-1</sup>) and PLANT + MB (20 mg kg<sup>-1</sup>) (scale bar: 1000 μm).

**e.** Immunofluorescence images of HIF- $\alpha$  and CD31 of tumors after treated with Nit, PLANT or PLANT + MB. **f.** Tumor images after the treatment of PBS, Nit, Tk and PLANT + Nit. **g.** Tumor images after the treatment of PBS, MB, Tk and PLANT + MB. **h.** Body weight curves of *in vivo* therapy during treatment with PBS, Nit, Tk and PLANT + Nit. **i.** H&E staining of mice tumor after 15 day of treatment with PBS, Nit, Tk and PLANT + Nit. **j.** Bioluminescence intensity of luciferase-expressed CT26 peripheral blood cells at 10th day during Nit, PLANT and PLANT + MB treatments. **k.** Semi-quantitative analysis of pulmonary bioluminescence intensity for Nit, PLANT and PLANT + MB treatment groups.

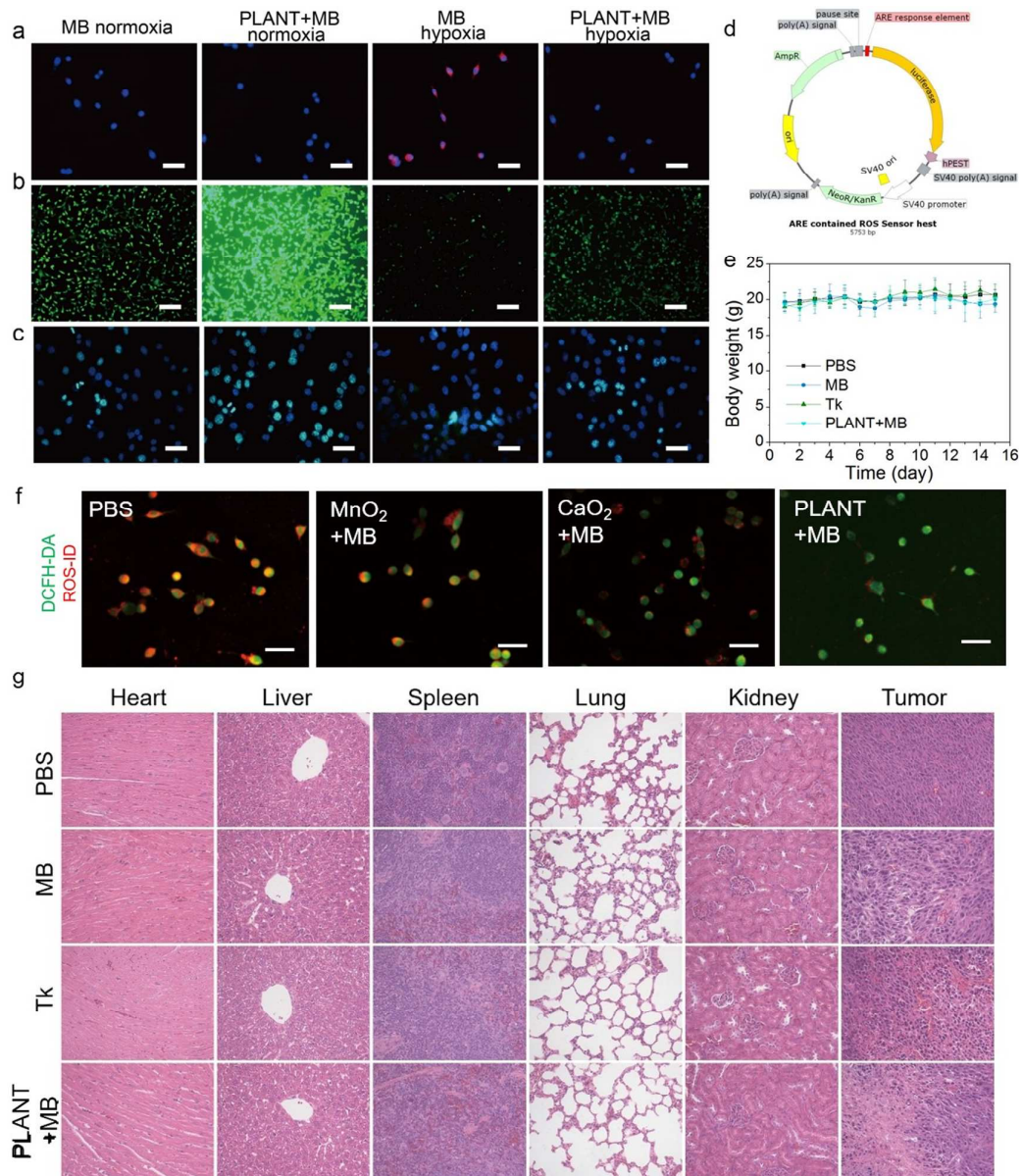


**Figure S12.** The therapeutic effect of PLANT combined with in inhibiting CT26 tumor growth. **a.** CLSM images of intracellular hypoxia indicated by ROS-ID hypoxia probe after 660 nm light irradiation (scale bar 50  $\mu$ m). **b.** CLSM images of DCFH-DA assay after 660 nm light irradiation. **c.** CLSM images of TUNEL assay after 660 nm light irradiation (scale bar 50  $\mu$ m). **d.** Plasmid profile of the ROS sensor with oxidative stress responsive elements driven expression of fast-degraded luciferase proteins. **e.** Body weight curves of *in vivo* therapy during treatment with PBS, MB, Tk and PLANT + MB. **f.** DCFH-DA and ROS-ID staining of CT26 cancer cells after treated

with  $\text{MnO}_2$  + MB,  $\text{CaO}_2$  + MB and PLANT + MB (scale bar 50  $\mu\text{m}$ ). **g.** H&E staining of mice tumor after 15 day of treatment with PBS, MB, Tk and PLANT + MB.

**Table S1. Detailed Information of Differential Metabolites Associated Pathway.**

Differential metabolites among PBS, PLANT + light and PLANT + dark treated mice tumor were analyzed with Reactome database. Changes of reactions in the pathway was listed.

Pathway name	Reactions	Reactions	Entities	Entities
	total	found	pValue	FDR
SLC-mediated transmembrane transport	184	56	1.11E-16	1.02E-13
Transport of vitamins, nucleosides, and related molecules	33	16	3.87E-12	1.65E-09
SLC transporter disorders	65	17	5.37E-12	1.65E-09
Nucleotide salvage	21	16	1.90E-10	4.37E-08
Transport of nucleosides and free purine and pyrimidine bases across the plasma membrane	11	11	3.22E-10	5.93E-08
Disorders of transmembrane transporters	87	23	8.87E-10	1.36E-07
Metabolism	2045	593	1.36E-09	1.78E-07
Metabolism of amino acids and derivatives	269	68	2.81E-09	3.23E-07
Transport of small molecules	430	143	3.19E-09	3.25E-07
Transport of bile salts and organic acids, metal ions and amine compounds	66	20	2.20E-08	2.02E-06
Nucleobase catabolism	58	49	2.93E-08	2.43E-06
Neurotransmitter release cycle	36	12	1.05E-07	7.95E-06
Purine salvage	11	8	4.68E-07	3.32E-05

Metabolism of nucleotides	135	95	5.15E-07	3.35E-05
Ketone body metabolism	11	7	5.75E-07	3.51E-05
Free fatty acid receptors	5	2	7.04E-07	4.01E-05
Pyrimidine catabolism	17	13	1.24E-06	5.95E-05
Organic cation/anion/zwitterion transport	12	5	1.24E-06	5.95E-05
Urea cycle	8	6	1.24E-06	5.95E-05
Organic cation transport	9	4	3.83E-06	1.71E-04
Base excision repair	87	16	3.98E-06	1.71E-04
Defective SLC27A4 causes ichthyosis prematurity syndrome (IPS)	1	1	4.19E-06	1.72E-04
Pyrimidine biosynthesis	6	5	5.95E-06	2.26E-04
Synthesis of ketone bodies	8	5	5.95E-06	2.26E-04
Metabolism of carbohydrates	214	76	6.56E-06	2.33E-04
Synthesis, secretion, and inactivation of Glucagon-like Peptide-1 (GLP-1)	7	1	6.65E-06	2.33E-04
Organic anion transporters	9	5	7.24E-06	2.46E-04
Pentose phosphate pathway (hexose monophosphate shunt)	20	12	9.72E-06	3.11E-04
Incretin synthesis, secretion, and inactivation	14	2	1.10E-05	3.40E-04
Na <sup>+</sup> /Cl <sup>-</sup> dependent neurotransmitter transporters	15	8	1.55E-05	4.65E-04
Metabolism of polyamines	38	18	2.16E-05	6.27E-04
Amino acid synthesis and interconversion (transamination)	32	7	2.44E-05	6.84E-04
G alpha (q) signalling events	29	5	3.11E-05	8.38E-04

Pyrimidine salvage	10	8	3.13E-05	8.44E-04
Nicotinate metabolism	29	17	3.56E-05	9.26E-04
Nicotinamide salvaging	12	7	3.88E-05	9.70E-04
Transport of fatty acids	2	1	4.13E-05	9.91E-04
Nucleobase biosynthesis	23	16	5.09E-05	1.22E-03
Digestion	24	6	5.56E-05	1.28E-03
Transport of inorganic cations/anions and amino acids/oligopeptides	75	21	6.14E-05	1.41E-03
Metabolism of ingested SeMet, Sec, MeSec into H <sub>2</sub> Se	10	2	6.70E-05	1.48E-03
Digestion and absorption	30	10	1.06E-04	2.24E-03
Cytosolic sulfonation of small molecules	24	6	1.15E-04	2.41E-03
Base-Excision Repair, AP Site Formation	44	9	1.24E-04	2.49E-03
Purine catabolism	28	24	1.33E-04	2.66E-03
Metabolism of vitamins and cofactors	200	62	1.59E-04	3.19E-03
Sphingolipid de novo biosynthesis	30	17	1.89E-04	3.59E-03
Fatty acyl-CoA biosynthesis	24	11	1.89E-04	3.59E-03
Transmission across Chemical Synapses	107	24	2.19E-04	3.79E-03
Synthesis of GDP-mannose	3	3	2.20E-04	3.79E-03
5-Phosphoribose 1-diphosphate biosynthesis	2	2	2.20E-04	3.79E-03
RUNX3 regulates YAP1-mediated transcription	3	1	2.23E-04	3.79E-03
Sulfur amino acid metabolism	28	9	2.30E-04	3.92E-03

Sphingolipid metabolism	61	24	2.50E-04	4.25E-03
Intestinal absorption	6	4	2.84E-04	4.54E-03
alpha-linolenic (omega3) and linoleic (omega6) acid metabolism	25	5	2.91E-04	4.66E-03
Class A/1 (Rhodopsin-like receptors)	143	14	2.95E-04	4.72E-03
Histidine catabolism	8	5	3.27E-04	4.91E-03
Linoleic acid (LA) metabolism	10	2	3.69E-04	5.53E-03
Pyruvate metabolism and Citric Acid (TCA) cycle	29	16	3.77E-04	5.65E-03
Metabolism of fat-soluble vitamins	33	15	3.77E-04	5.65E-03
Utilization of Ketone Bodies	3	2	4.44E-04	6.21E-03
YAP1- and WWTR1 (TAZ)-stimulated gene expression	9	1	6.34E-04	8.87E-03
RORA activates gene expression	10	2	6.99E-04	9.79E-03
Gluconeogenesis	26	16	7.08E-04	9.91E-03
Integration of energy metabolism	65	15	7.71E-04	1.00E-02
Vitamin B2 (riboflavin) metabolism	5	3	7.77E-04	1.01E-02
Cleavage of the damaged pyrimidine	17	8	7.77E-04	1.01E-02
Depyrimidination	34	8	7.77E-04	1.01E-02
Defective SLC2A2 causes Fanconi-Bickel syndrome (FBS)	1	1	8.25E-04	1.07E-02
Degradation of cysteine and homocysteine	14	6	1.01E-03	1.31E-02
Glycogen metabolism	38	13	1.10E-03	1.32E-02
Phase I - Functionalization of compounds	99	19	1.19E-03	1.43E-02
Fructose catabolism	5	4	1.24E-03	1.48E-02
Adrenaline signalling through	1	1	1.28E-03	1.54E-02

Alpha-2 adrenergic receptor				
Citric acid cycle (TCA cycle)	14	7	1.30E-03	1.56E-02
Coenzyme A biosynthesis	7	4	1.42E-03	1.56E-02
Amine Oxidase reactions	6	4	1.62E-03	1.78E-02
Purine ribonucleoside monophosphate biosynthesis	17	11	1.77E-03	1.95E-02
Pyrophosphate hydrolysis	2	2	1.83E-03	2.01E-02
Defective SLC16A1 causes symptomatic deficiency in lactate transport (SDLT)	1	1	1.83E-03	2.01E-02
Metabolism of steroids	234	36	1.91E-03	2.02E-02
G alpha (i) signalling events	147	36	1.94E-03	2.02E-02
Peptide hormone metabolism	60	2	2.02E-03	2.02E-02
Amine ligand-binding receptors	15	9	2.05E-03	2.05E-02
Synthesis of very long-chain fatty acyl-CoAs	12	5	2.05E-03	2.05E-02
mRNA decay by 3' to 5' exoribonuclease	3	2	2.07E-03	2.07E-02
Regulation of cholesterol biosynthesis by SREBP (SREBF)	52	4	2.11E-03	2.11E-02
Mitochondrial biogenesis	36	5	2.18E-03	2.18E-02
Transcriptional activation of mitochondrial biogenesis	32	4	2.22E-03	2.22E-02
Creatine metabolism	6	2	2.33E-03	2.29E-02
Surfactant metabolism	27	3	2.35E-03	2.29E-02
Synthesis of substrates in N-glycan biosynthesis	48	19	2.54E-03	2.29E-02
Digestion of dietary carbohydrate	13	3	2.60E-03	2.34E-02

Glycogen synthesis	22	5	2.60E-03	2.34E-02
The canonical retinoid cycle in rods (twilight vision)	25	3	2.86E-03	2.57E-02
Fructose metabolism	7	5	2.89E-03	2.57E-02
Histidine, lysine, phenylalanine, tyrosine, proline and tryptophan catabolism	53	9	3.17E-03	2.57E-02
Selenoamino acid metabolism	33	8	3.18E-03	2.57E-02

---

**Table S2. Detailed Information About Animals Experiments.** All animal experiments were performed on 6-week-old female Balb/c mice.

Experiment	Material	Dose (per mice)	n	Method of administration	Method of irradiation
<i>In vivo</i> tumor targeting	PLANT with folic acid	0.4 mg	4	<i>i.v.</i>	non
	PLANT without folic acid	0.4 mg	4	<i>i.v.</i>	non
<i>Ex vivo</i> fluorescence imaging	PLANT with folic acid	0.4 mg	4	<i>i.v.</i>	non
	PLANT without folic acid	0.4 mg	4	<i>i.v.</i>	non
Tissue clearing	PLANT	0.4 mg	4	<i>i.v.</i>	155 mWcm <sup>-2</sup> 2 min
Anaphylaxis	PLANT	0.4 mg	4	<i>i.v.</i>	non
	Tk	0.4 mg	4	<i>i.v.</i>	non
	OVA	0.8 mg	4	<i>i.v.</i>	non
Blood biochemistry analysis	PLANT	0.4 mg	4	<i>i.v.</i>	non
	Tk	0.4 mg	4	<i>i.v.</i>	non
Metabonomics	PLANT	0.4 mg	4	<i>i.v.</i>	155 mWcm <sup>-2</sup> 2 min
	PLANT	0.4 mg	4	<i>i.v.</i>	non

ROS generation	PLANT+M	0.4 mg +	4	<i>i.v.</i>	155
	B	0.1 mg			mWcm <sup>-2</sup> 2 min
O <sub>2</sub> generation and <i>in vivo</i> anti-cancer therapy	MB	0.1 mg	6	<i>i.v.</i>	155
					mWcm <sup>-2</sup> 2 min
	PLANT	0.4 mg	6	<i>i.v.</i>	155
					mWcm <sup>-2</sup> 2 min
Anti-angiogenesis therapy	PLANT+M	0.4 mg +	6	<i>i.v.</i>	155
	B	0.1 mg			mWcm <sup>-2</sup> 2 min
	Nit	2.5 mg	6	<i>p.o.</i>	non
Mechanism of PLANT in sensitizing Nit	PLANT	0.4 mg	6	<i>i.v.</i>	155
					mWcm <sup>-2</sup> 2 min
	PLANT+Nit	0.4 mg + 2.5 mg	6	<i>i.v. + p.o.</i>	155
					mWcm <sup>-2</sup> 2 min
Mechanism of PLANT in sensitizing Nit	Nit	2.5 mg	5	<i>p.o.</i>	non
	PLANT	0.4 mg	5	<i>i.v.</i>	155
					mWcm <sup>-2</sup> 2 min
Mechanism of PLANT in sensitizing Nit	PLANT+Nit	0.4 mg + 2.5 mg	5	<i>i.v. + p.o.</i>	155
					mWcm <sup>-2</sup> 2 min